



**UPCONVERSION LUMINESCENCE PROPERTIES OF Ga₂O₃: Yb³⁺, Er³⁺
NANOPARTICLES: EFFECTS OF CALCINATION TEMPERATURE AND DOPANT
CONCENTRATION**

Ayşe DULDA^{1,*}

¹ Department of Material Science and Nanotechnology Engineering, Engineering Faculty, Yeditepe University,
İstanbul, Turkey

ABSTRACT

Fluorides despite been the most widely studied host matrices for many upconversion nanoparticles are usually hygroscopic and are of limited use. Hence, explorations of new upconversion host materials that will be more efficient in practical application are still active areas of research. In this study, applicability of Ga₂O₃ as a host matrix for upconversion luminescence was investigated under near infrared (980 nm) excitation. XRD and FT-IR analysis indicate that changes in the calcination temperature and dopant ion concentration lead to crystal phase transformation of nanoparticles from β-Ga₂O₃ to cubic Yb₃Ga₅O₁₂ garnet. Resulting changes in crystal field and sites symmetries alter the behaviour of upconversion. Accordingly, tunable green, red and infrared luminescences were observed.

Keywords: Upconversion luminescence, β-Ga₂O₃, Near infrared (980 nm) excitation

1. INTRODUCTION

Recently, upconversion nanoparticles (UCNPs) with high upconversion luminescence (UCL) efficiencies have widely been investigated because of their potential applications in upconversion lasers, molecular detection, biological labelling, therapeutics, and volumetric three-dimensional displays, [1-2]. UCNPs typically comprise of the lanthanides (Ln³⁺) doped on a hosting material. Ln³⁺ ions are active centres that provide required energy levels for multiple photon additions to occur [3]. Among Ln³⁺ ions, erbium (Er³⁺) ion has widely been investigated [4-5]. However, its practical application is limited due to its low absorption cross section around the 980nm [1]. The luminescence properties of Er³⁺ ion can be improved around 980nm when codoped with another Ln³⁺ ion such as Ytterbium (Yb³⁺) ion (used as sensitizer) that has large absorption cross-section around 980nm and can transfer the absorption energy to a neighbouring Er³⁺ ion [6-7]. Er-Yb codoped UCNPs have received considerable research attention [1-2, 8-9]. UCL efficiencies of the Er-Yb codoped UCNPs depend on several factors such as concentration of Er³⁺ and Yb³⁺ dopants, homogeneous distributions of Er³⁺ and Yb³⁺ ions, sintering temperature, hosting material, etc. The effects of the concentrations of Er³⁺ and Yb³⁺ ions in some hosting materials such as CaF₂ [1], LiTaO₃ [8] and Gd₂O₃ [10] on the upconversion emission have been investigated. Green, red (upconversion) and near infrared emission intensities were found to increase with increasing Yb concentration in Yb-Er codoped CaF₂ material [1]. Also, enhanced green and red upconversion emissions were reported when concentrations of Er³⁺ ions were increased in Er doped LiTaO₃ [8]. In general, emission intensities have been found to increase with the increase in concentrations of the Yb and Er ions in the codoped system up to an appropriate dopant concentration [1, 8, 10]. However, higher concentration can induce cross relaxations between dopants which subsequently reduce the efficiency of the UCL [11]. Apart from the dopant concentration, the calcination temperature is another influencing factor on the UCL efficiency. Increasing the calcination temperature can result to improved crystallinity and larger grain size which reduces surface defects

that can result to lower non-radioactive loss. Hence, the UCL efficiency is improved by increasing calcination temperature.

The hosting material is another important factor that affect the UCL efficiency. An ideal hosting material should have low lattice phonon energy so as to minimize non-radiative loss and maximize the radiative emission. Although, halides such as chlorides, bromides and iodides could be suitable hosting material due to their low phonon energies of less than 300 cm^{-1} , they are usually hygroscopic and are of limited use [12]. Similarly, oxides generally show higher chemical stabilities compared to halides with relatively high phonon energies ($\sim 500\text{ cm}^{-1}$). Many oxides have been investigated as hosting materials such as Gd_2O_3 [10], LiTaO_3 [8] and ZnO [13]. Since only few high efficiency UCNPs hosting materials have been found to be suitable for practical applications, current researches still concentrate largely on seeking new hosting materials. Gallium oxides (Ga_2O_3) despite been used as hosting materials in many phosphorous applications due to their optical properties, very few researchers have investigated them as hosting materials in upconversion process [14-16]. It has been established that Ga_2O_3 can be a promising hosting material for upconversion and photodynamic therapy. The crystal structure of Ga_2O_3 can be classified in five different polymorphs: alpha (α); beta (β); gamma (γ); delta (δ) and sigma (ϵ) [17, 18]. The β phase is more suitable for upconversion because of the wide band gap [18]. In this research, β - Ga_2O_3 is employed as a novel hosting material due to its advantages stated above. The aim of the research is to investigate the effect of changing concentrations of Ln^{3+} ions and calcination temperature on the co-doped $\text{Yb-Er-Ga}_2\text{O}_3$ powders. Crystalline phases, morphologies, elemental compositions and photoluminescence emissions of the samples were analysed and the results were discussed in the subsequent section.

2. MATERIALS AND METHODS

2.1. Chemicals

GaCl_3 (ultra dry 99,999% Abcr), YbCl_3 (Ytterbium(III) chloride anhydrous, beads, -10 mesh, 99.99%, Sigma Aldrich), ErCl_3 (Erbium(III) chloride anhydrous, beads, -10 mesh, 99.99%, Sigma Aldrich), sodium hydroxide (reagent grade, $\geq 98\%$, pellets anhydrous Sigma Aldrich), PEG-6.000 (poly(ethylene glycol), Mw = 6,000, Merck), were used without further purification.

2.2 Procedure

Yb^{3+} and Er^{3+} codoped Ga_2O_3 nanocrystals were prepared by a precipitation method in the presence of surfactant (PEG-6000). In a typical synthesis, 1 mmol ($\%79,5\text{ GaCl}_3$, $\%20\text{ YbCl}_3$, $\%0,5\text{ ErCl}_3$) and 5 mmol PEG-6000 were dissolved in 57 mL deionized water to form a clear solution under magnetic stirring. 2M sodium hydroxide (NaOH) was added quickly into this solution and pH of the solution reached to 7 at room temperature. Resulting fluffy (Ga:Yb:Er)OOH precipitates were collected with centrifugation at 15000 rpm and dried at room temperature for 24 h. The as-prepared precipitates were calcined under various temperatures at $750\text{ }^\circ\text{C}$ and $1150\text{ }^\circ\text{C}$ for an hour in air atmosphere.

2.3 Instrumentations

The crystalline phases of the samples were determined by powder X-Ray Diffraction method using a Bruker D8 Advance X-ray diffractometer with $\text{CuK}\alpha$ radiation. A scan rate of $2\theta\text{ }^\circ/\text{min}$ was set over the range of $10 - 70^\circ$. The morphological characterization of the samples was monitored using scanning electron microscopy (Zeiss LS-10 GmbH, Germany) equipped with EDX (Bruker 123 eV). Fourier transform infrared (FT-IR) spectra were recorded on a Tensor 27 spectrometer (Bruker Optics, Wissembourg, France). It was equipped with a horizontal attenuated total reflectance (ATR) accessory composed of a ZnSe. The emission spectra were measured using a CNI MDL-H-975 Model diode laser operating at 975 nm with an output power of 5W as excitation source with a Princeton

Instruments SP2500i model monochromator. The luminescence spectra of prepared samples in the infrared and visible regions were measured by Acton series ID441-C Model InGaAs and SI 440 detectors. All measurements were carried out at room temperature.

3. RESULTS AND DISCUSSIONS

3.1 Morphology and Crystallinity

Sizes and morphologies of Ga₂O₃:Yb,Er nanoparticles were observed by SEM microscopy and, elemental analysis was conducted with Energy Dispersive X-ray Spectroscopy (EDX) as shown in Fig. 1. The-prepared nanoparticles show nearly spherical morphology and their sizes are uniformly distributed with an average diameter of ~10 nm. After being calcined at 750 °C, Ga₂O₃:Yb,Er nanoparticles preserve their particle sizes and morphologies (Figure 1(a) -1(b)).

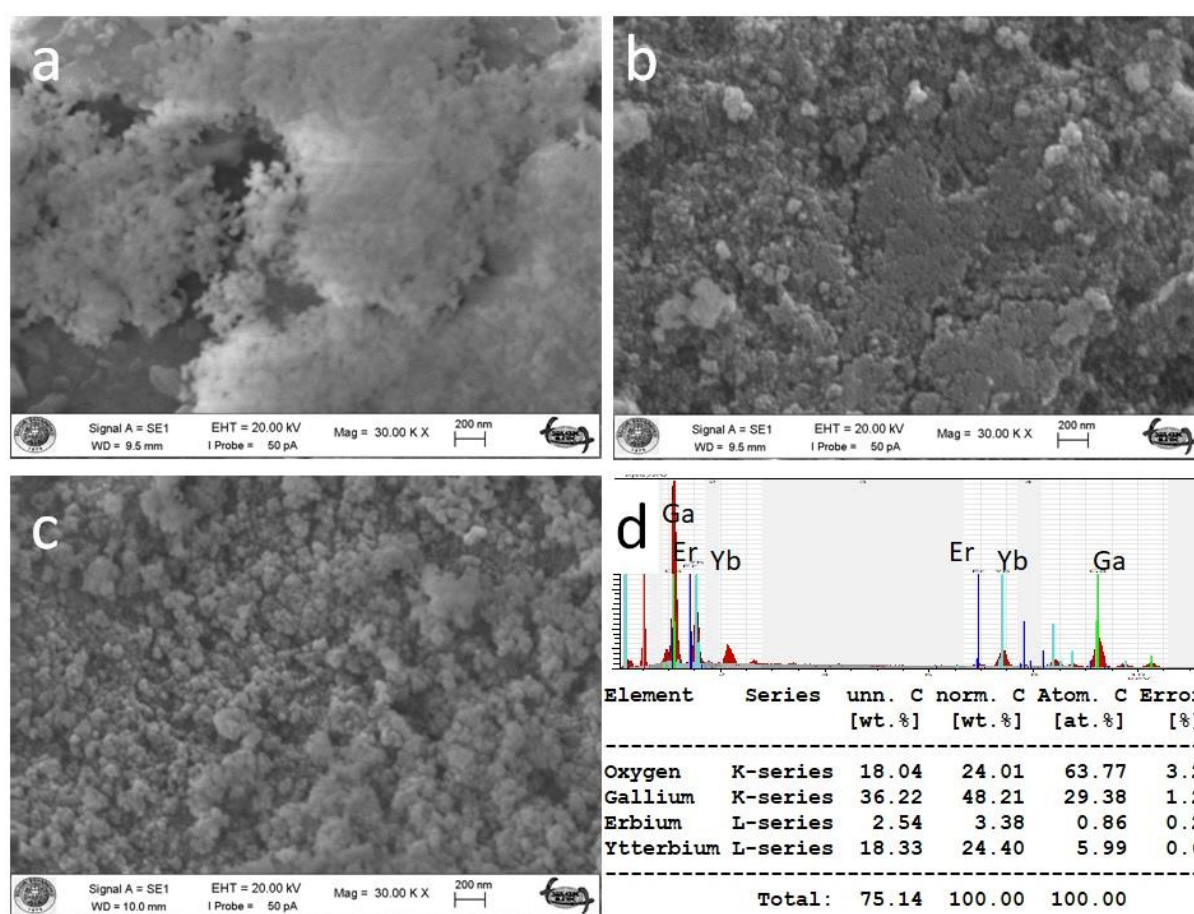


Figure 1. SEM images of Ga₂O₃: Yb, Er nanocrystals a) before calcinations, b) calcined at 750 °C, and c) calcined at 1150 °C. d) EDX spectrum of Yb20-750 sample.

As the calcination temperature is raised to 1150 °C, nanoparticles agglomerate slightly and the average particle size is raised to ~20 nm (Fig. 1(c)). Experimental parameters such as dopant ion concentration and calcination temperature are listed in Table I and samples are labelled accordingly. The elemental composition of Yb20-1150 sample was analysed by the EDX spectroscopy and the result showed that the intended composition was not obtained. (Fig. 1(d)). This could be due to miscalibration of the chemical solution concentration.

Table 1. Experimental parameters for dopant ion concentration and calcination temperature. (*Er0.5 – 750 and Yb20-750 samples have same compositions)

Sample	Temperature	Er Concentration (mol%)	Yb Contraction (mol%)
Er0.5 - 750	750 °C	0.5	20
Er1.0 - 750	750 °C	1.0	20
Er1.5 - 750	750 °C	1.5	20
Er2.0 - 750	750 °C	2.0	20
Yb20-750	750 °C	0.5	20
Yb1-1150	1150 °C	0.5	1
Yb10 - 1150	1150 °C	0.5	10
Yb20 - 1150	1150 °C	0.5	20

Crystalline structures and phase purities of Ga₂O₃:Yb,Er samples prepared through the hydrolysis with NaOH in the presence of PEG-6000 were examined by XRD. Fig. 2. shows the XRD patterns of the Ga₂O₃:Yb,Er samples.

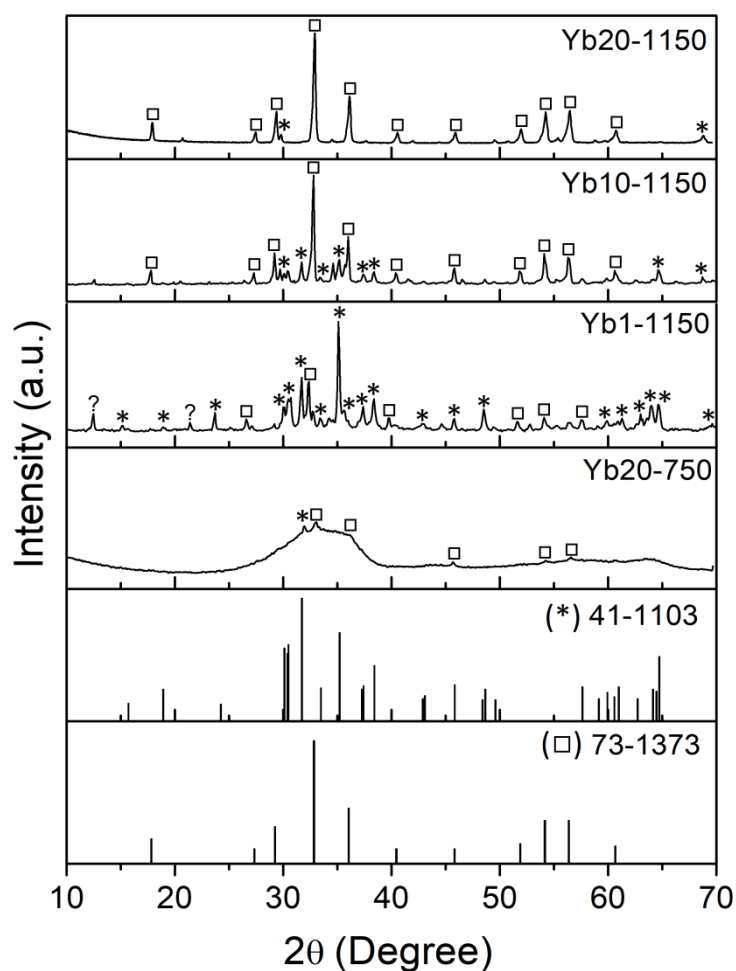


Figure 2. XRD diffraction patterns of Ga₂O₃: Yb, Er nanocrystals. β-Ga₂O₃(JCPDS card No. 41-1103) and Yb₃Ga₅O₁₂ garnet phase (JCPDS card No. 73-1373) marked with (*) and (□), respectively.

It can be observed that XRD pattern of Yb20-750 show a broad band (indicating amorphous phase) containing mostly the cubic structured $\text{Yb}_3\text{Ga}_5\text{O}_{12}$ garnet phase (JCPDS card No. 73-1373) except the monoclinic polymorph of the $\beta\text{-Ga}_2\text{O}_3$ (JCPDS card No. 41-1103) at $2\Theta=31,83^\circ$. While monoclinic polymorph of the $\beta\text{-Ga}_2\text{O}_3$ is marked with asterisk (*), cubic structured $\text{Yb}_3\text{Ga}_5\text{O}_{12}$ garnet phase is marked with square symbol (\square). It is clear to see sharp and narrow peaks indicating high crystallinity of all samples calcined at 1150°C . Although most of peaks in the Yb1-1150 sample correspond to $\beta\text{-Ga}_2\text{O}_3$ few peaks correspond to $\text{Yb}_3\text{Ga}_5\text{O}_{12}$ garnet phase observed even at 1% of Yb concentration. Yb10-1150 sample exhibits combination of peaks that correspond to either the $\beta\text{-Ga}_2\text{O}_3$ or the cubic $\text{Yb}_3\text{Ga}_5\text{O}_{12}$ garnet patterns. There is also an unknown peak at $2\Theta=21,40^\circ$ shown by question mark. As Yb ion concentration is increased to 10%, number of peaks belonged to $\text{Yb}_3\text{Ga}_5\text{O}_{12}$ garnet phase is increased. The peaks pattern of the Yb20-1150 sample, which corresponds to the cubic $\text{Yb}_3\text{Ga}_5\text{O}_{12}$ garnet, affirmed to the assertion that a phase transfer has occurred when the Yb concentration is raised from 1% ($\beta\text{-Ga}_2\text{O}_3$ phase) to 20% (cubic $\text{Yb}_3\text{Ga}_5\text{O}_{12}$ garnet phase).

To confirm crystalline sizes of our samples obtained from SEM images of Fig. 1, an estimate of the sizes was computed from the XRD data using equation (1) in Wejrzanowski et al [19] and [20]. After most peaks in the XRD spectrum were approximately fitted, estimated average particle sizes for the Yb20-750 and Yb20 - 1150 samples were found to be around 10 and 20 nm respectively.

3.2 FT-IR Analysis

The FT-IR spectrum of the Yb20-750, Yb1-1150, Yb10-1150 and Yb20-1150 samples is shown in Fig. 3.

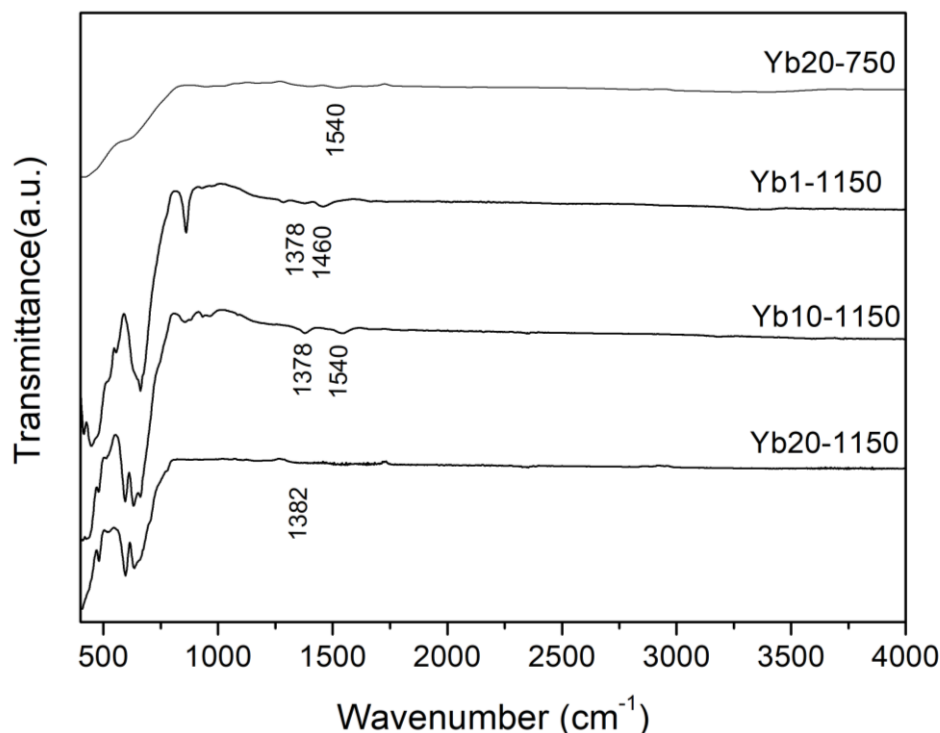


Figure 3. FTIR spectra of Er^{3+} and Yb^{3+} codoped Ga_2O_3 nanoparticles calcined at 750°C and 1150°C

It can be observed that for all the samples, no clear peak exists between ~ 1540 and 4000 cm^{-1} . This indicates successful removal of PEG-6000 from surfaces of the samples during the calcination procedure. Small peaks between ~ 1378 and $\sim 1540\text{ cm}^{-1}$ could not be identified. If we assume that the peaks in this range belonged to the organic group, these peaks could have disappeared by increasing temperature to 1150°C . For the Yb20-750 sample, bands at 935 cm^{-1} and 626 cm^{-1} were observed

which can be attributed to the bending mode of Ga-OH and stretching modes of Ga-O bonds, respectively. As stated in the previous section, Yb1-1150 sample exhibits β -Ga₂O₃ phase. The β -Ga₂O₃ lattice has C2/m symmetry as Ga atoms in the lattice are exhibiting tetrahedral (GaO₄) and octahedral (GaO₆) coordination [21, 22]. Peaks at 860 cm⁻¹ and 661 cm⁻¹ for the Yb1-1150 sample can be assigned to stretching modes of GaO₄ and GaO₆ respectively. The spectrum of the Yb10-1150 sample indicates peaks at 860 cm⁻¹, 661 cm⁻¹, 595 cm⁻¹, and 480 cm⁻¹. Peaks 661 cm⁻¹, 595 cm⁻¹, and 480 cm⁻¹ are attributed to stretching modes of GaO₄ in the garnet structure. It can be observed that, unlike in the Yb1-1150 sample, the peak at 860 cm⁻¹ in the Yb10-1150 sample is reduced. This is due to higher Yb³⁺ concentration in the Yb10-1150 sample that results in structural disorder of the tetrahedra which induced the replacement of Yb³⁺ ion in the dodecahedral sites. This peak is reduced as the Yb³⁺ concentration increases. As it has been proposed by Mc Devitt, that the crystal volume effects only the Yb-O in series garnet structures.

And, since both the tetrahedra and the octahedra share edges with the dodecahedra, increasing the crystal volume will result as the distortion of the tetrahedral through the expansion of the dodecahedra. For the Yb20-1150 sample, observed peaks at 659 cm⁻¹, 634 cm⁻¹, 595 cm⁻¹, and 480 cm⁻¹ are attributed to the stretching mode of the GaO₄ in the garnet structure. This agrees with the XRD data that indicates the presence of cubic Yb₃Ga₅O₁₂ garnet structure. Observed peaks at 480, 595, 634 cm⁻¹ in both the Yb10-1150 and Yb20-1150 spectrum match with the stretching mode of Yb-O bond with cubic Yb₃Ga₅O₁₂ garnet reported by McDevitt et al. [23, 24].

3.3 Upconversion Luminescence

Photoluminescence study of all samples was performed based on the variation of their calcination temperature and dopant concentration. Figure 4 shows the room temperature visible emission spectra of Yb20-750 and Yb20-1150 samples.

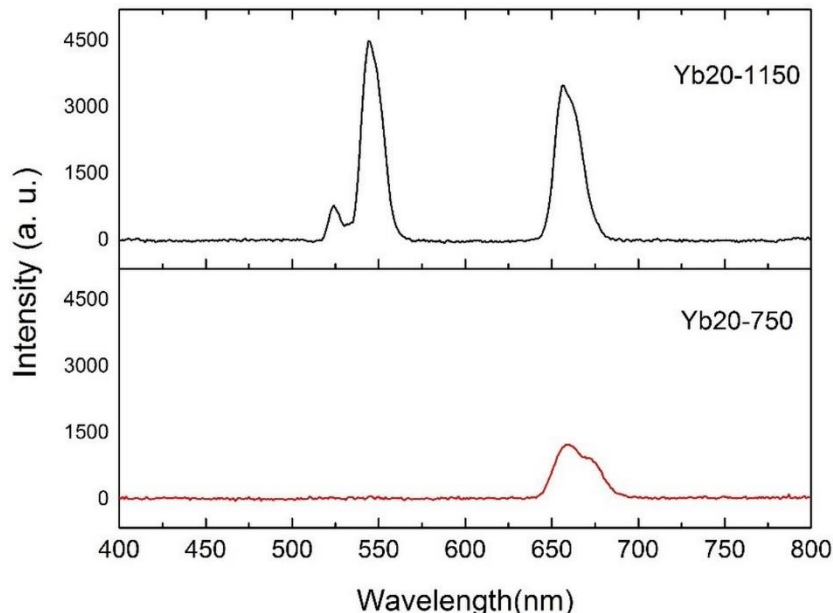


Figure 4. The room temperature emission spectra ($\lambda_{\text{ex}}=980$ nm) of Er³⁺ and Yb³⁺ codoped Ga₂O₃ nanoparticles calcined at a) 750 °C and b) 1150 °C. The concentration of Er³⁺ and Yb³⁺ ions was 0,5 and 20mol%, respectively.

Red emission with low intensity was observed at lower synthesis temperature (Yb20-750 sample), while enhanced intensities of both red and green emissions were observed at higher synthesis temperature (Yb20-1150 sample). This behaviour can be explained using the XRD analysis discussed

in the previous section. From the figure 2, the Yb20-750 sample indicates both amorphous (non-crystalline) β - Ga_2O_3 and $\text{Yb}_3\text{Ga}_5\text{O}_{12}$ garnet phases are present due to the inadequacy of the calcination temperature. While Yb20-1150 sample indicated pure crystalline $\text{Yb}_3\text{Ga}_5\text{O}_{12}$ garnet phase. The increased crystallinity will inevitably leads to the enhanced emission.

Figure 5(a) and Figure 5(b) show the room temperature visible and infrared emission spectra of Yb20 – 750, Er1.0 – 750, Er1.5 – 750, and Er2.0 – 750 samples when excited at 980 nm. The emission spectrum shows that only red emission was observed around 650 nm. Red emission intensity decreased as the concentration of Er^{3+} ion is increased. The production of the red emission occurs via transitions between ${}^4\text{F}_{9/2} \rightarrow {}^4\text{I}_{15/2}$ levels and it can be enhanced by the population of ${}^4\text{F}_{9/2}$ state either through the Excited State Absorption (ESA) or Energy Transfer Upconversion (ETU) or both (Figure 6).

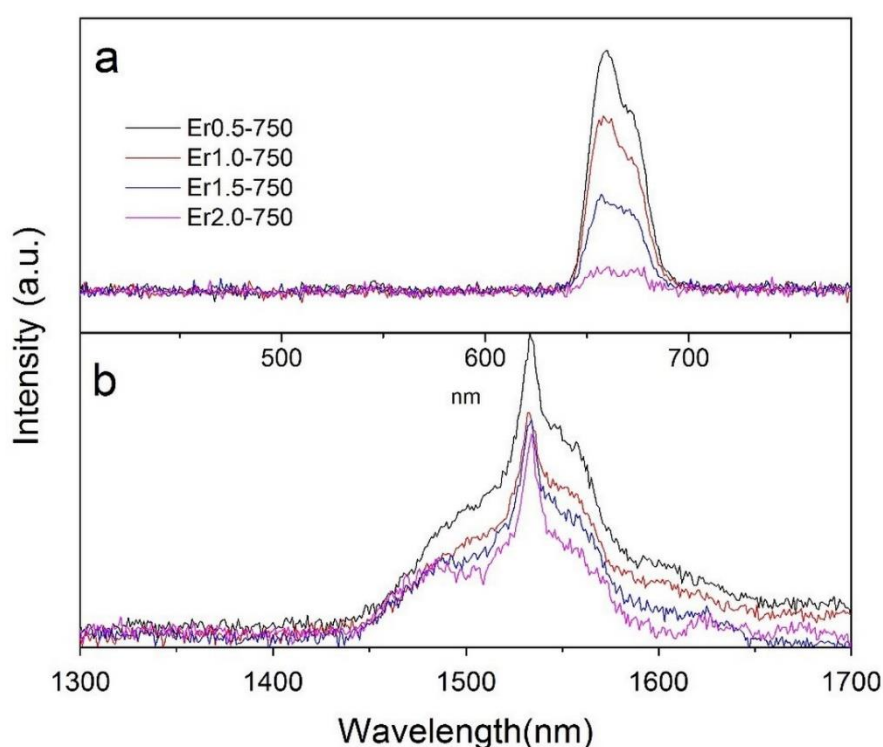


Figure 5. The room temperature (a) visible and (b) infrared emission spectra ($\lambda_{\text{ex}}=980$ nm) of Er^{3+} and Yb^{3+} codoped Ga_2O_3 nanoparticles calcined at 750 °C. The concentration of Er^{3+} ion was changed to be 0.5mol%, 1mol%, 1.5mol% and 2mol% at constant 20mol% Yb^{3+} ion concentration.

The population of ${}^4\text{F}_{9/2}$ level well established in the literature could be due to three major mechanisms: (1) Non-radiative relaxations bypassing the ${}^2\text{H}_{3/2}$ and ${}^4\text{S}_{3/2}$ states; (2) cross relaxations between any two excited Er^{3+} ions that allows ${}^4\text{F}_{7/2} \rightarrow {}^4\text{F}_{9/2}$ and ${}^4\text{F}_{9/2} \leftarrow {}^4\text{I}_{11/2}$ energy transfer; and (3) direct population from ${}^4\text{I}_{13/2}$ level through the non-radiative decay of ${}^4\text{I}_{11/2} \rightarrow {}^4\text{I}_{13/2}$ [25, 26]

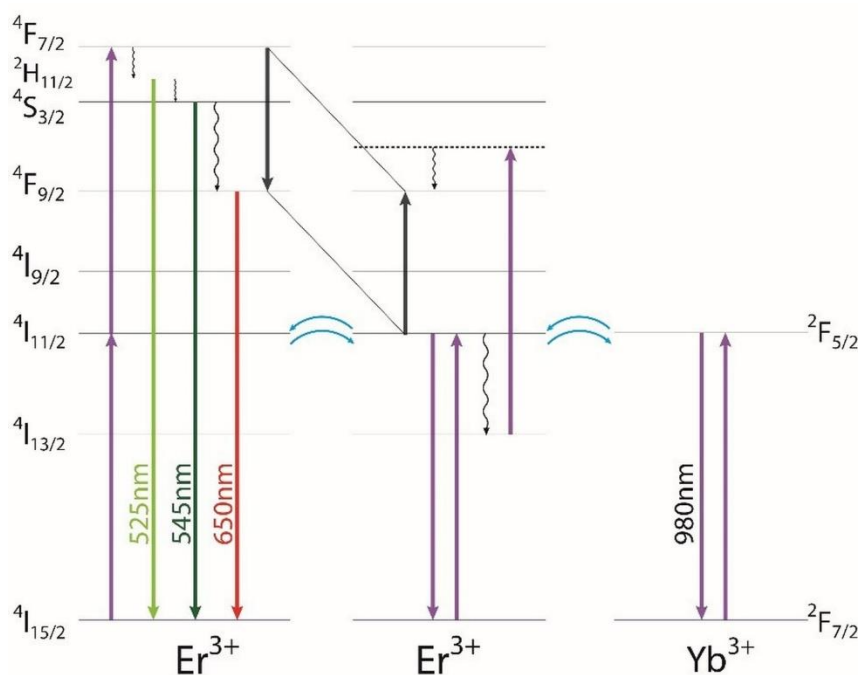


Figure 6. Schematic representation of upconversion mechanism in Yb^{3+} and Er^{3+} codoped Ga_2O_3 nanocrystals.

It can be deduced from Figure 5(a) that cross-relaxations and the nonradiative decay of ${}^4\text{I}_{11/2} \rightarrow {}^4\text{I}_{13/2}$ are relatively efficient in these samples based on the observed red emission. It is believed that the efficiency of the cross-relaxation mechanism is expected to raise with increasing Er^{3+} concentration since the average distance between dopant ions are decreased. Also, the increasing Er^{3+} ion concentration can be resulted in higher probability of the nonradiative decay of ${}^4\text{I}_{11/2} \rightarrow {}^4\text{I}_{13/2}$. This is because; larger surface areas of smaller nanoparticles may contain a higher number of Er^{3+} ions. When Er^{3+} ions are coupled to OH^{-1} ions (with high vibration energy of 3600 cm^{-1}) on the surface, ions can be relaxed to ${}^4\text{I}_{13/2}$ level non-radiatively by bridging the gap between ${}^4\text{I}_{11/2} \rightarrow {}^4\text{I}_{13/2}$ [27]. However, our FTIR spectrum (Figure 3) shows that, there are no significant OH^{-1} ions existing on the surface of nanoparticles. Also, the samples emission spectra show that only red and infrared emissions were obtained for all concentrations as emission intensities are decreased by increasing Er^{3+} concentration. This can be attributed to the raise in crystal defects as the lanthanide concentration increases. If the Er^{3+} is incorporating into the crystal, and therefore the Er^{3+} ion size ($0,0881\text{nm}$) is relatively larger than the Ga^{3+} ($0,062\text{nm}$), lattice distortion occurs. This inevitably makes samples to have quenching centres (traps). When an excited luminescent centre is in the vicinity of any of these traps, the excited energy can be transferred easily to the trap non-radiatively. As concentrations of Er^{3+} ions increase, the lattice distortion increases and the quenching also increases which ultimately result as weaker upconversion luminescence. In addition, the increase of the full width at the half maximum (FWHM) of the infrared emission band (${}^4\text{I}_{11/2} \rightarrow {}^4\text{I}_{15/2}$) can also be indicative of the increasing lattice distortion as the Er^{3+} concentration increases (Figure 5(b)). This is because; the increased FWHM indicates presences of Er^{3+} ions located at diverse sites [28, 29].

Figure 7 shows the room temperature visible and infrared emission spectra of Yb1-1150, Yb10-1150 and Yb20-1150 samples.

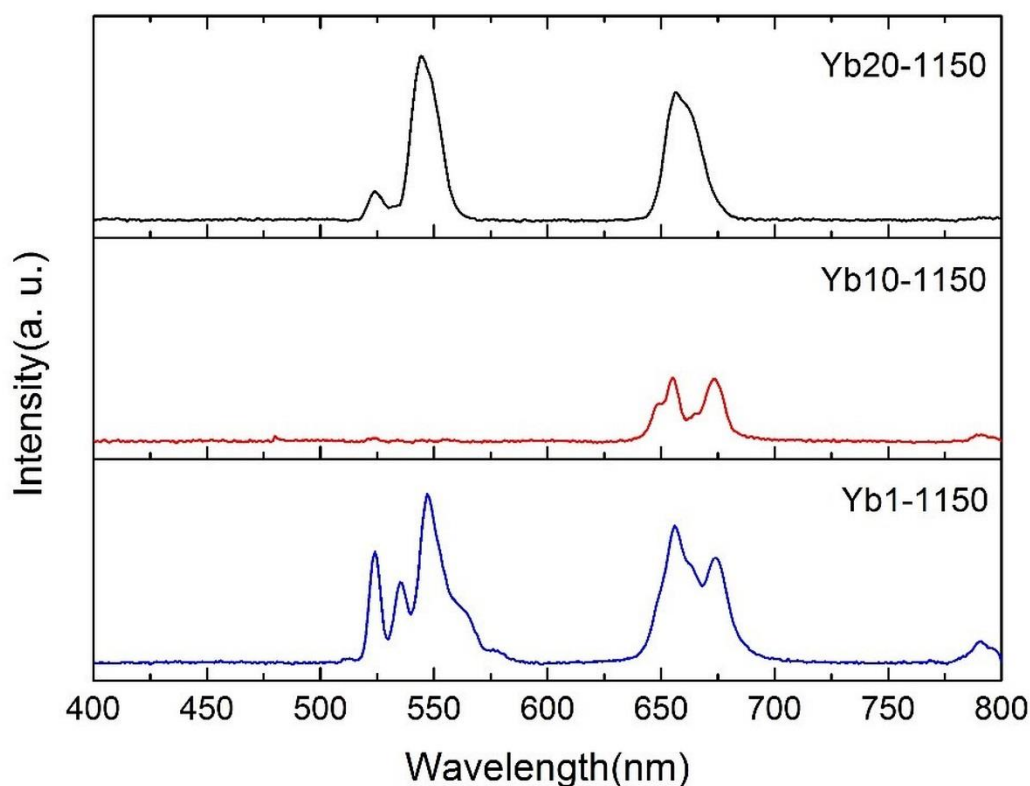


Figure 7. The room temperature emission spectra ($\lambda_{ex}=980$ nm) of Er³⁺ and Yb³⁺ codoped Ga₂O₃ nanoparticles calcined at 1150 °C. The concentration of Yb³⁺ ion was changed to be 1mol%, 10mol%, and 20 mol% at constant 0.5mol% Er³⁺ ion concentration.

Green, red, and infrared emissions were observed at various intensities when the samples were excited with 980 nm. Green emissions are centered at 525 and 545 nm which can be assigned to $^2H_{11/2} \rightarrow ^4I_{15/2}$ and $^4S_{3/2} \rightarrow ^4I_{15/2}$ transitions respectively.

Red emissions are centered at 655 and 675nm which are attributed to $^4F_{9/2} \rightarrow ^4I_{15/2}$ transitions. Infrared emission centered at 791 nm is assigned to $^2I_{11/2} \rightarrow ^4I_{15/2}$ transition. For the Yb1-1150 sample, green, red and infrared luminescences were observed. When the concentration of the Yb³⁺ ion is increased in case of the Yb10-1150 sample, overall luminescence intensities decrease and the green emission disappeared. The disappearance of the green emission could be due to the presence of a secondary phase highlighted in the XRD and FT-IR analysis of the same sample in the previous section. It has been suggested that reduced intensities could be due to aggregations of donor Yb³⁺ ions which may act as trapping centers at higher Yb³⁺ concentrations thereby dissipating energy non radiatively [16]. However, when the concentration of Yb³⁺ ion is further increased as in the case of Yb20-1150 sample, visible luminescence intensities (green and red emissions) are enhanced and infrared emission disappeared. Hence, reduced intensities (Yb10-1150 sample) and increased intensities (Yb20-1150 sample) of green and red emission can best be explained with the effect of the host matrix on the upconversion luminescence efficiency. It has been established that luminescence efficiencies of Er³⁺ doped materials are greatly influenced by the energy migration and the crystal field symmetry of Er³⁺ in the host matrix [29]. And also, relative intensities of same emissions change when the site symmetry changes. For the Yb10-1150 sample, existence of multiple phases imply that the host matrix contains the combination of multiple sites symmetries (octahedral- β -Ga₂O₃ and dodecahedral-

Yb₃Ga₅O₁₂ garnet sites). This causes the differentiation of the admixture of even and odd parity states, which changes the electric dipole component of the transitions, thereby amounting to reduced emissions [17]. For the Yb20-1150 sample, since only Yb₃Ga₅O₁₂ garnet phase exists, increased emissions and the disappearance of the infrared emission can be attributed to the pure garnet phase which is more suitable for efficient upconversion process. It was reported that in the garnet structure, the dodecahedral is the active emitting site while in β-Ga₂O₃, octahedral is the active site. Also, the dodecahedral shows stronger green emission and the octahedral site shows stronger infrared emission [30]. Hence, the increased green emission in the Yb20-1150 sample is due to dodecahedral site symmetry. Similarly, the reduction of the infrared emission intensity from Yb1-1150 to Yb20-1150 implies the gradual transformation from β-Ga₂O₃ to the Yb₃Ga₅O₁₂ garnet phase. In addition, due to the new phase, the distance between ions (and possibly phonon energies) would be different which will ultimately affect the upconversion spectrum.

3.4 CIE Colour Coordinates Analysis

Figure 8 shows the CIE 1931 chromaticity diagram of the Yb³⁺ and Er³⁺ codoped Ga₂O₃ nanoparticles and the points 1, 2, 3, and 4 show the chromaticity coordinates of the Yb1-1150, Yb10-1150, Yb20-1150 and Yb20-750 samples.

CIE 1931

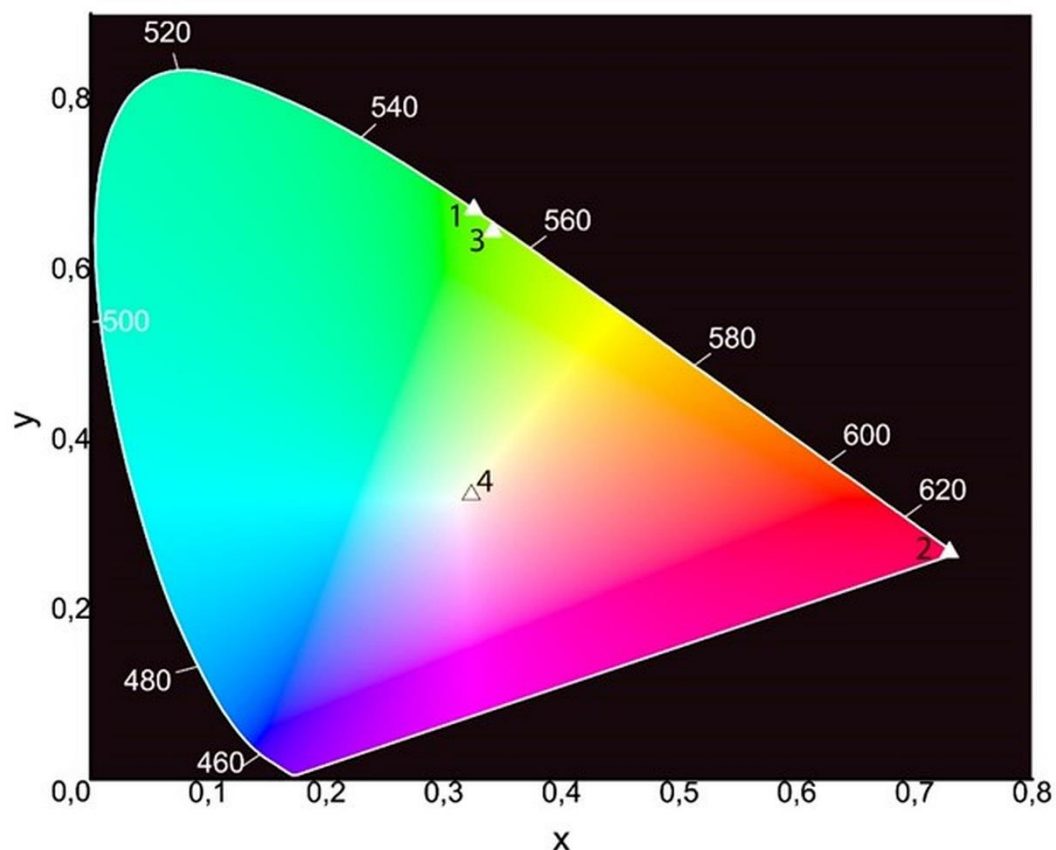


Figure 8. The CIE 1931 chromaticity coordinates of the Yb1-1150, Yb10-1150, Yb20-1150 and Yb20-750 samples.

The chromaticity coordinates (x, y) are (0.341, 0.643), (0.729, 0.267), (0.325, 0.669) and (0.323, 0.334) respectively. They are calculated based on their corresponding upconversion emission spectra shown in Figure 4 and Figure 7. Usually, changing the dopant concentration results as intensity

variations of visible emissions that will be reflected as a gradual shift in the chromaticity coordinates. However, our results indicate that tunable emission color can be observed by changing dopant concentration and calcination temperature. This implies that, crystal field and symmetries of sites in Ga₂O₃ host are very sensitive to doping and heat treatment due to its unique crystal structure.

4. CONCLUSION

In this research, upconversion luminescence properties of Yb and Er codoped β -Ga₂O₃ have been investigated both in the visible and infrared range under 980 nm excitation. Results of the effect of changing the dopant concentration and the calcination temperature on upconversion luminescence properties have been demonstrated. It was observed that higher Er concentration resulted in lower red and infrared emissions. Also, higher calcination temperature led to enhanced crystallinity and visible luminescence intensities. Furthermore, crystal phase transformation from monoclinic β -Ga₂O₃ to cubic Yb₃Ga₅O₁₂ garnet phase was found to be sensitive to the change in the Yb ion concentration. Accordingly, changes in the crystal field and sites symmetries yield tunable visible emissions.

ACKNOWLEDGEMENTS

This work was supported by the TUBITAK under Project no. 113M899.

REFERENCES

- [1] Liu Z, Mei B, Song J, & Yi G. Influence of Yb Concentration on the Optical Properties of CaF₂ Transparent Ceramics Codoped with Er and Yb. *J Am Ceram Soc* 2015; 98(12): 3905-3910.
- [2] Wu S, ... & Shen J. Polypeptide-Functionalized NaYF₄: Yb³⁺, Er³⁺ Nanoparticles: Red-Emission Biomarkers for High Quality Bioimaging Using a 915 nm Laser. *ACS Appl Mater Interfaces* 2014; 6(20): 18329-18336.
- [3] Auzel F. Upconversion and anti-stokes processes with f and d ions in solids. *Chem. Rev.* 2004; 104(1): 139-174.
- [4] Kapoor R, Friend CS, Biswas A, & Prasad PN. Highly efficient infrared-to-visible energy upconversion in Er³⁺: Y₂O₃. *Opt. Lett.* 2000; 25(5): 338-340.
- [5] Dymshits OS, Loiko PA, Skoptsov NA, Malyarevich AM, Yumashev KV Zhilin AA ... & Bogdanov K. Structure and upconversion luminescence of transparent glass-ceramics containing (Er, Yb)₂(Ti, Zr)₂O₇ nanocrystals. *J Non Cryst Solids* 2015; 409: 54-62.
- [6] Lu S, Yang Q, Zhang B, & Zhang H. Upconversion and infrared luminescences in Er³⁺/Yb³⁺ codoped Y₂O₃ and (Y_{0.9}La_{0.1})₂O₃ transparent ceramics. *Opt Mater* 2011; 33(5): 746-749.
- [7] Dwivedi Y, Mishra K, & Rai S. B. Synthesis of bright multicolor down and upconversion emitting Y₂Te₄O₁₁: Er; Yb nanocrystals. *J. Alloys Compd.* 2013; 572: 90-96.
- [8] Shi L, Shen Q, & Qiu Z. Concentration-dependent upconversion emission in Er-doped and Er/Yb-codoped LiTaO₃ polycrystals. *J Lumin.* 2014; 148: 94-97.
- [9] Zhang J, Wang S, Rong T, & Chen L. Upconversion luminescence in Er³⁺ doped and Yb³⁺/Er³⁺ codoped yttria nanocrystalline powders. *J Am Ceram Soc* 2004; 87(6): 1072-1075.

- [10] Li H, Song S, Wang W, & Chen K. In vitro photodynamic therapy based on magnetic-luminescent Gd₂O₃: Yb, Er nanoparticles with bright three-photon up-conversion fluorescence under near-infrared light. Dalton Trans. 2015; 44(36): 16081-16090.
- [11] Li X, Wang R, Zhang F, & Zhao D. Engineering homogeneous doping in single nanoparticle to enhance upconversion efficiency. Nano Lett 2014; 14(6): 3634-3639.
- [12] Zhou J, Liu Q, Feng W, Sun Y, & Li F. Upconversion luminescent materials: Advances and applications. Chem. Rev. 2014; 115(1): 395-465.
- [13] Wei X, Wang W, & Chen K. ZnO: Er, Yb, Gd particles designed for magnetic-fluorescent imaging and near-infrared light triggered photodynamic therapy. J. Phys. Chem. C 2013; 117(45): 23716-23729.
- [14] Miyata T, Nakatani T & Minami T. Gallium oxide as host material for multicolor emitting phosphors. J Lumin 2000; 87: 1183-1185.
- [15] Fleischer M. Höllbauer L. Born E. & Meixner H. Evidence for a Phase Transition of β -Gallium Oxide at Very Low Oxygen Pressures. J Am Ceram Soc 1997; 80(8): 2121-2125.
- [16] Nogales E. García J. A. Méndez B. Piqueras J. Lorenz K. & Alves E. Visible and infrared luminescence study of Er doped β -Ga₂O₃ and Er₃Ga₅O₁₂. J Phys D Appl Phys. 2008; 41(6): 065406.
- [17] Biljan T. Gajović A. & Meić Z. Visible and NIR luminescence of nanocrystalline β -Ga₂O₃:Er³⁺ prepared by solution combustion synthesis. J Lumin, 2008: 128(3); 377-382.
- [18] Taş AC Majewski P. J. & Aldinger F. Synthesis of gallium oxide hydroxide crystals in aqueous solutions with or without urea and their calcination behavior. J Am Ceram Soc 2002; 85(6): 1421-1429.
- [19] Wejrzanowski T. Pielaszek R. Opalińska A. Matysiak H. Łojkowski W. & Kurzydłowski K. J. Quantitative methods for nanopowders characterization. Appl. Surf. Sci. 2006; 253(1): 204-208.
- [20] Pielaszek R. Analytical expression for diffraction line profile for polydisperse powders. In Applied Crystallography in Proceedings of the XIX Conference, 2004: Singapore. World Scientific, USA: pp. 43-50.
- [21] S He H. Orlando R. Blanco M. A. Pandey R. Amzallag E. Baraille I. & Rérat M. (2006). First-principles study of the structural, electronic, and optical properties of Ga₂O₃ in its monoclinic and hexagonal phases. Physical Review B 2006; 74(19); 195123.
- [22] Dulda A. Morphology Controlled Synthesis of α -GaO(OH) Nanoparticles: Thermal Conversion to Ga₂O₃ and Photocatalytic Properties. Adv. Mater. Sci. Eng. 2016; 2016: 1-9.
- [23] McDevitt N. T. Infrared lattice spectra of rare-earth aluminum, gallium, and iron garnets. JOSA 1969; 59(9): 1240-1244.
- [24] Papagelis K. Arvanitidis J. Vinga E. Christofilos D. Kourouklis G. A. Kimura H. & Ves S. Vibrational properties of (Gd_{1-x}Y_x)₃Ga₅O₁₂ solid solutions. J. Appl. Phys. 2010; 107(11): 113504.

- [25] Vetrone F. Boyer J. C. Capobianco J. A. Speghini A. & Bettinelli M. (2004). Significance of Yb³⁺ concentration on the upconversion mechanisms in codoped Y₂O₃:Er³⁺,Yb³⁺ nanocrystals. *J. Appl. Phys.* 2004; 96: 661-667
- [26] Sun Y. Chen Y. Tian L. Yu Y. Kong X. Zhao J. & Zhang H. Controlled synthesis and morphology dependent upconversion luminescence of NaYF₄:Yb,Er nanocrystals. *Nanotechnology* 2007; 18(27): 275609.
- [27] Snoeks E. Kik P. G. & Polman A. Concentration quenching in erbium implanted alkali silicate glasses. *Opt Mater* 1996; 5(3): 159-167.
- [28] Sun H. Hu L. Wen L. Duan Z. Zhang J. & Jiang Z. Effect of chloride ions' introduction on structural, thermal stability, and spectroscopic properties in Yb³⁺ Er³⁺- codoped germanate-bismuth-lead glasses. *JOSA B* 2005; 22(12): 2601-2609.
- [29] Chen SY, Ting CC, & Li CH. Fluorescence enhancement and structural development of sol-gel derived Er³⁺-doped SiO₂ by yttrium codoping. *J Mater Chem* 2002; 12(4): 1118-1123.
- [30] Zong L. Xu P. Ding Y. Zhao K. Wang Z. Yan X. ... & Xing X. Y₂O₃: Yb³⁺/Er³⁺ Hollow Spheres with Controlled Inner Structures and Enhanced Upconverted Photoluminescence. *Small* 2015; 11(23): 2768-2773.